Nanoscale

Accepted Manuscript

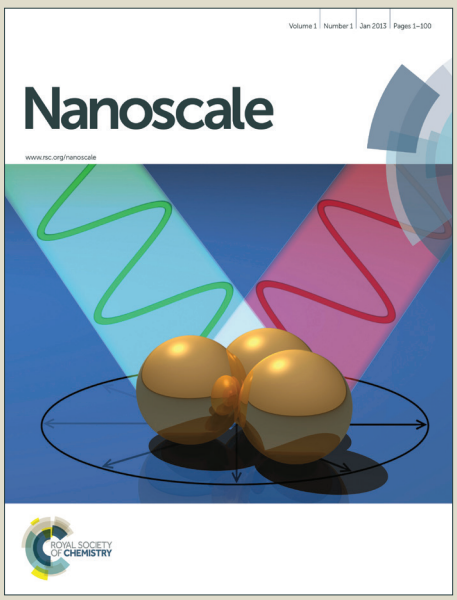

ROYAL SOCIETY OF CHEMISTRY

www.rsc.org/nanoscale

ARTICLE TYPE www. rsc.org/xxxxxx | XXXXXXXX

Injection and waveguiding properties in SU8 nanotubes for sub-wavelength regime propagation and nanophotonics integration

John Bigeon,[a] Nolwenn Huby,[a,*] Jean-Luc Duvail,[b] and Bruno Bêche [a,c]

Received Xth XXXXXXXXXX 20XX, Accepted Xth XXXXXXXXX 20XX
First published on the web Xth XXXXXXXXXX 200X
DOI: 10.1039/b000000x

We report photonic concepts related to injection and sub-wavelength propagation in nanotubes, an unsual but promising geometry for highly integrated photonic devices. Theoretical simulation by finite domain time-dependent (FDTD) method was first used to determine the features of direct light injection and sub-wavelength propagation regime within nanotubes. Then, the injection into nanotubes of SU8, a photoresist used for integrated photonics, was successfully achieved by using polymer microlensed fibers with sub-micronic radius of curvature, as theoretically expected from FDTD simulations. The propagation losses into single SU8 nanotube were determined by using a comprehensive set-up and a protocol for optical characterization. The attenuation coefficient has been evaluated at 1.25 dB/mm by a cut-back method transposed to such nanostructures. The mechanisms responsible for losses in nanotubes were identified with FDTD theoretical support. Both injection and cut-back method developed here are compatible with any sub-micronic structures. This work on SU8 nanotubes suggest broader perspectives for future nanophotonics.

1 Introduction

Miniaturization offers great opportunities for integrated photonic devices. However, the comprehension of optical behaviors at the nanoscale and the ability to confine light in structures with sub-wavelength diameters require further developments. Due to their high aspect ratio, the nanofibers (nanowires or nanotubes) have emerged in nanophotonics as a new class of sub-micronic structures[1]. Among the various optical components that have been reported, integration of components based on these 1D-nanostructures have already demonstrated their interest in all-optical active switching[2], optical detection of gas mixtures[3], reduction of laser threshold[4], nonlinearity effects[5] or supercontinuum aspects[6]. Due to processing in liquid-phase, organic materials offer opportunities to elaborate original systems at a reasonable cost. In addition, organic components present a large range of accessible optical properties by the versatility of their chemical structures. Literature on nanophotonics mainly reports on inorganic[4] and polymer nanowires[7,8], while polymer nanotubes present a lack of investigations despite their great potential. Indeed, in nanophotonics as in conventional optical fiber, the tubular geometry may extend the prospective field of waveguide behavior. By numerical analysis, Almeida *et al.*[9] have shown that the tubular geometry of nanotube can uniquely confine part of the light in the lowest refractive index area, the core of the nanotube. In parallel, Zhao *et al.*[10] have theoretically demonstrated the modulation of field and dispersion properties in nanotube. As we report in our previous theoretical letter, waveguiding of light in such nanotube allows the control of propagation characteristics[11]. Finally, the hollow area into the core of waveguide, slab, rib, and cylindrical as nanotube, is a unique feature to control and modulate passive guiding properties with the intrinsec and specific leaky modes familly existence[12]. The literature proposes different methods to synthesize polymer nanofibers[1–6], but few of them include the processing of polymer nanotubes. The stretching of micronic tubules by melting was reported[13] but it requires a high temperature step, which can be a drawback. Alternatively, polymeric nanotubes have been elaborated by a wetting template method[14]. This technique achieves a fine control of the dimensions, a low-cost of fabrication, and the opportunity for a large-scale production.

Besides the effective fabrication of 1D-nanostructures, the injection of light in sub-micrometric objects is a milestone for integrated optics. In conventional optical fibers, the coupling can be performed through a guided mode by a prism and by grating side couplers[15]. But these techniques can not be easily transposed at the nanoscale for nanofibers. The main strategy used up-to-now in nanophotonics is based on evanescent coupling of stretched fibers to nanofibers with a relatively good efficiency (around 95 %)[16]. However, this method requires a substantial length of coupling (*i.e.* 3 μm)[16], and it does not

[a] *Institut de Physique de Rennes, Université de Rennes 1, CNRS UMR 6251, Rennes, France*
[*] *E-mail: Nolwenn.huby@univ-rennes1.fr*
[b] *Institut des Matériaux de Nantes Jean Rouxel, Université de Nantes, CNRS UMR 6502, Nantes, France*
[c] *Institut universitaire de France, IUF, Paris, France*

allow to control precisely the characteristics of the incident light. A recent study[17] proposes alternatively the formation of *Escherichia coli* bio-waveguides with light injection made from a tapered fiber.

Here, we propose a global approach to inject light and to investigate waveguiding behavior within nanotubes. First the simulation by finite domain time-dependent (FDTD) method was used to anticipate how direct light injection and sub-wavelength propagation regime can take place into such structures according to optical and geometrical features. The SU8 polymer was selected, because it is a widely-used epoxy based negative photoresist, and commonly used in integrated photonics, due to its excellent characteristics for micronic waveguides[18]. SU8 polymer presents large refractive index compared to most organics and polymers. This large refractive index enhances the confinment in light waveguiding. Additionally, the different viscosity of SU8 in liquid phase is a central advantage for nanowire and nanotube processing by the template strategy. It can be mentioned that doping SU8 photoresist with dyes or nanoparticules is accessible for tuning the refractive index and introduce photoactive media[19]. Here, we addressed the challenge of direct injection of light into nanotubes by developing an innovative set-up. Based on FDTD simulation and experimental protocol, the efficiency of the coupling between a microlensed fiber with sub-micronic radius of curvature and the nanotube, as well as the propagation losses within the nanotube were determined and discussed in details. These SU8 polymer nanotubes can be considered as a prototypal building-blocks for integrated nanophotonics.

2 Numerical study of coupling phenomena

To anticipate the injection of light in nanotube, a numerical 3D FDTD simulation was performed with Meep freeware[20]. FDTD simulation has already proved accuracy to study optical sub-wavelength propagation in nanostructures[21,22]. The model contains a microlensed fiber (final curvature radius of 500 nm) aligned in direction of free-standing SU8 nanotube with refractive indexes of $n_{microlens} = 1.54$ and $n_{SU8} = 1.56$ at 675 nm. Inner and external diameters of SU8 nanotube were fixed at 120 nm and 240 nm respectively for a length of 5 μm. The cylindrical geometry of the microlens has been chosen to coincide with the tubular symmetry of synthesized SU8 nanotubes, as reported below. Thereby, the energy overlap integral between the injecting microlens and the SU8 nanotubes is maximized. The computational domain is discretized into a uniform orthogonal 3-dimensional mesh with cubic cell size of 10 nm side surrounded by perfectly matched layers. A y-polarized laser source at 675 nm (FWHM =12 nm) is launched inside the microlens. Figure 1a is a top-view of the power density. The presence of standing wave patterns along the axis of nanotube attests the coupling phenomena between SU8 nanotube and microlensed fibers. They are due to interferences between propagating light and reflections at the output endfacet. This phenomenon has been already established on waveguiding silica nanowires[23]. Projection of power density inside the nanotube along Ox on figure 1a corroborates the period of standing waves: $P = \frac{\lambda}{2n_{eff}} \cong 332$ nm from our previous theoretical work[11]. Figure 1b present 3D and orthogonal views (*i.e.* along Oyz plan) of the optical power mode HE_{11} ($P_{PowerDensity}$) inside the SU8 nanotube. It highlights the significant confinment of power density inside the hollow region, the maximum of light propagating in the wall of the nanotube with an extension of the density power of 50 nm in air. To obtain more information of the power distribution in the optical mode inside SU8 nanotube, we calculate the confinment factor Γ_1 as the fractional power inside the central hollow region Γ_{hollow} over the central hollow region and dielectric region and outer cladding $\Gamma_{hollow+dielec+outer}$. In a symmetrical way, we calculate the confinment factor Γ_2 as the fractional power inside the central hollow region and dielectric region $\Gamma_{hollow+dielec}$ over the central hollow region and dielectric region and outer cladding $\Gamma_{hollow+dielec+outer}$. So, confinment factor Γ_1 and Γ_2 and the ratio of these confinment factors, Γ_{ratio}, were defined as following:

$$\Gamma_1 = \frac{\Gamma_{hollow}}{\Gamma_{hollow+dielec+outer}} = \frac{\iiint\limits_{hollow} P_{PowerDensity}\,\mathrm{dydz}}{\iiint\limits_{hollow+dielec+outer} P_{PowerDensity}\,\mathrm{dydz}},$$

$$\Gamma_2 = \frac{\Gamma_{hollow+dielec}}{\Gamma_{hollow+dielec+outer}} = \frac{\iiint\limits_{hollow+dielec} P_{PowerDensity}\,\mathrm{dydz}}{\iiint\limits_{hollow+dielec+outer} P_{PowerDensity}\,\mathrm{dydz}},$$

$\Gamma_{ratio} = \frac{\Gamma_1}{\Gamma_2}$.

Confinment factors of $\Gamma_1 = 0.0457$, $\Gamma_2 = 0.1721$, $\Gamma_{ratio} \cong 0.266$ have been evaluated here with numerical study for the SU8 nanotube. These values confirm the relative confinment inside the hollow region and also the substantial part of evanescent field of propagating light. The ratio is in proper agreement with extrapolated data of ratio of confinment factors in the literature[10] and underline an interesting aspect for sensing applications.

The normalized intensity distribution along the Oy axis was also investigated from the output endface[22]. Figure 1c presents the transversal profile of the propagative spot at three distances from the nanotube end noted x_0, x_1 and x_2 (as located on figure 1a). At the end face of nanotube, the light spreads like a source point. Thus, as one moves away from the output facet of the nanotube, the profile significantly widens. This is a typical behavior of optical fiber.

A quantitative analysis of optical coupling can be performed by the determination of light power in the microlens and in the SU8 nanotube. The coupling efficiency (η) was determined as a function of the distance between the microlens and the SU8 nanotube and is presented on figure 1d. The maximum of coupling is logically obtained at x$\cong$ 0 μm, while

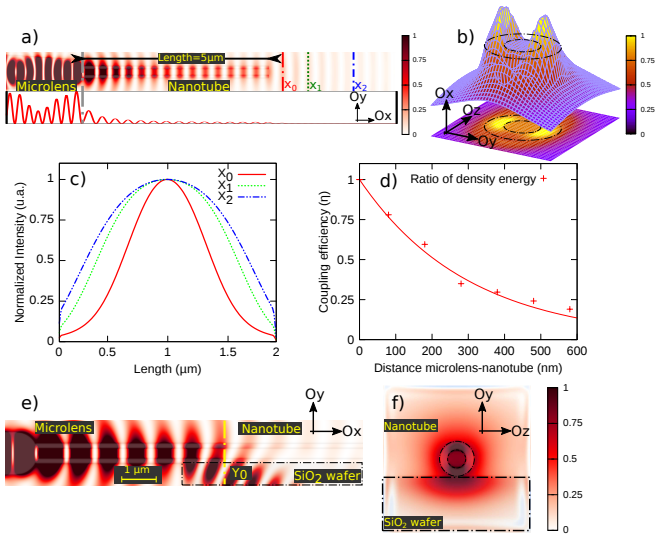

Fig. 1 Numerical FDTD investigation of light injection and coupling phenomena in nanotube a) Light power density and coupling between a SU8 nanotube and a microlens surrounded by air under laser source at 675 nm. b) Power density of the HE_{11} mode and 3D-view of the mode confirm the significant confinment of power density inside the hollow core. c) Transversal profiles of propagative light at three positions after the nanotube (reported in (a)). d) Coupling efficiency (η) as a function of the distance between microlens and nanotube. Light power density and coupling between a SU8 nanotube and a microlens on SiO_2 wafer along e) 0xy plane and f) Oyz plane.

the decay follows an exponential decrease law with the loss of half the power output the microlens after 200 nm. For integrated nanophotonics applications, the nano-waveguides are deposited on a substrate, most frequently SiO_2 wafer. In order to determine the role of the SiO_2 wafer, FDTD simulations of light propagation inside SU8 nanotube deposited on SiO_2 wafer were also performed. The resulting intensity profile is reported along Oxy plan (figure 1e) and for an orthogonal view located along Y_0 (figure 1f). Near the input side of SU8 nanotube, an important part of intensity is vanished inside the wafer. This can be compared with figure 1a for which the cladding is air. The respective refractive indexes of SiO_2 wafer and SU8 nanotube ($n_{SiO_2} = 1.45$ and $n_{SU8} = 1.56$) promote leakages of the light from the SU8 waveguides nanotubes to the wafer. It is emphasized that the reduction of diameter of the waveguide structure enhances this effect because a larger part of the propagating light extends outside the fiber. This weak confinement induces leakage inside the wafer but is still compatible with efficient propagation.

3 Synthesis of SU8 photoresist nanotubes

SU8 nanotubes were elaborated by the wetting template method[14], based on the wetting of an alumina nanoporous membrane (anodized aluminum oxide AAO) by the polymer in a liquid phase[24]. An impregnation of the 240 nm diameter pores from a commercially available 60 μm thick AAO membrane with a drop of SU8 2010 photoresist was performed. Once the membrane is impregnated over the entire thickness, a UV insolation (λ = 365 nm, 200 mJ/cm^2) provokes cross-linking of the polymer to get the solid form. A selective chemical etching by immersion in H_3PO_4 solution (25 % wt) releases SU8 nanotubes from the AAO. Finally, SU8 nanotubes were dispersed into isopropyl alcohol solution or distilled water and a drop of this suspension of SU8 nanotubes was deposited onto a clean SiO_2 wafer.

4 Results and Discussion

4.1 Structural characterization

Figure 2a displays scanning electron microscopy (SEM) images of SU8 nanotubes after release from the AAO membrane. No residual material and a smooth surface validate the fabrication process. SU8 nanotubes present regular and hollow end-facets, as highlighted by the inset of figure 2a. An inner diameter ranging between 90 and 130 nm was estimated from SEM study. In order to confirm the effective tubular aspect all along the nanotubes, a drop of isopropyl alcohol solution was spread on top of the sample after the UV exposition step. The flow of the liquid on the opposite side attested the tubular nature of the nanotubes. Additionally, it can be noted that the wetting template method tends to promote a smooth inner surface, as also shown in the literature[25]. It is important to emphasize the good mechanical robustness of the SU8 nanotubes. Indeed, no mechanical collapsing was observed by SEM imagery and it has been possible to manipulate them with a nanomanipulator. On figure 2a, the presence of several SU8 nanotubes strongly bended without mechanical damage demonstrates that they are quite flexible.
Atomic force microscopy (AFM) study has been performed to confirm the nanotube diameter. A selection of height profiles measured for a SU8 nanotube (figures 2b, 2c) shows that the external diameter of SU8 nanotubes ranges between 250 nm and 325 nm typically. This diameter dispersion is attributed to the inhomogeneity of the pore diameters of the AAO templates. A quite uniform roughness around 5 nm was measured along nanotubes and it confirms the smooth surface, a requirement to reduce intensity losses along the propagation.

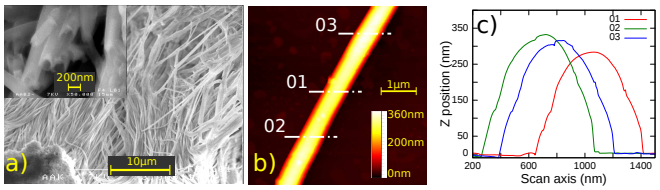

Fig. 2 a) SEM images of SU8 nanotubes fabricated by the wetting template after release from the AAO membrane. The inset shows the tubular aspect. b) AFM image of a single nanotube on a SiO_2 substrate. c) Height profiles corresponding to the three dashed lines on the nanotube.

4.2 Photonic characterization

The experimental setup developed in this work (figure 3) presents two innovative aspects : a protocol for direct injection in 1D nanostructures and a derived from the cut-back method for attenuation coefficient estimation in 1D nanostructures. The light injection is performed with single-mode microlensed polymer fibers (*Lovalite*). These microlensed fibers are mounted on piezo-electric nano-positioner (Pi-611-SF) in order to precisely control their positionning with 10 nm step in the three directions. A top-view display system consisting of a monochrome CCD camera (AVT GX1920), with pixels size of 4.54 μm associated with x40 and x100 optical lenses (numerical aperture 0.90, working distance 1 mm) permits the simultaneous control and optimization of the light injection in nanostructures. A similar set-up has already been developed to study sub-wavelength propagation in polymer nanowires [26]. After the removal of the AAO template by chemical etching, the nanotubes were dispersed in isopropyl alcohol and then dropped onto a SiO_2 wafer. This wafer was cleaved and the SU8 nanotubes located at the cleaved face were selected in order to facilitate the approach of the microlensed fiber.

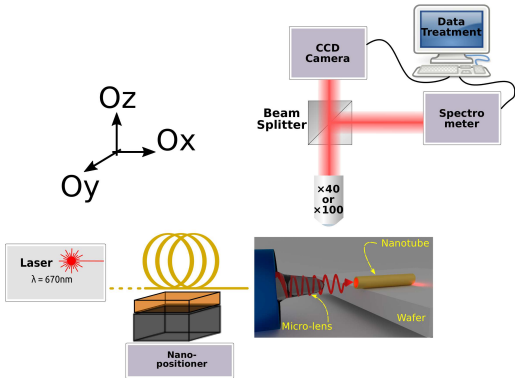

Fig. 3 Sketch of experimental direct injection. A microlensed fiber is mounted on piezo-electric nano-positioner. A top-view optical path allows the control of the approach of microlensed fiber and nanotube. The beam splitter leads to either a CCD camera or a spectrometer for optical analysis of coupling phenomena.

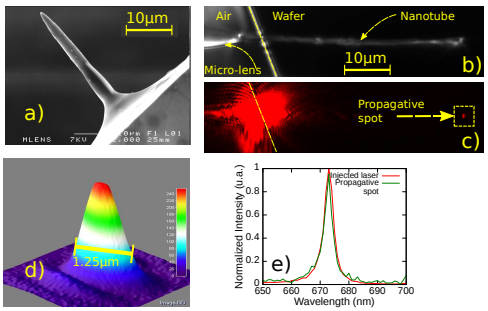

Fig. 4 a) SEM image of the microlensed polymer fiber for direct injection in nanotube. b) Top-view image by optical microscopy of the microlensed fiber positioned near the SU8 nanotube with cleaved face in dashed line. c) Same image under laser excitation at 675 nm. d) 3D-view of propagative spot after data treatment of the image in the square area of c). e) Spectral analysis in top-view of microlens lobe and propagative spot.

5 Results and discussion

5.1 Injection

The injection of light into nanowires and nanotubes was previously achieved by our group through an evanescent coupling [14]. However, the efficiency of this coupling is hardly controlled and the eventual contribution of the scattered light is a drawback for accurate measurements of the propagation features. For these reasons, the direct injection of light into individual nanotube is highly desired but of particular challenge. A visible laser light (λ=675 nm, FWHM= 12 nm) was used for light propagation in nanotube. Microlensed fibers present at their end a curvature radius of 500 nm as shown on figure 4a. Under laser excitation, they exhibit a light lobe of a few micrometers in diameter and a power of 121 $\pm$ 25 nW. Figure 4b presents the approach of the microlensed fiber near the SU8 nanotube under visible light. The microlens is manipulated by a piezo-system and located at a few micrometers of the nanotube. When the injection of light is effective, a spot at the opposite end of the nanotube is detected, as shown on figure 4c. The presence of the spot is the proof of a significant propagation into the SU8 nanotube. A 3D-view of this propagative spot is depicted on figure 4d allowing the estimation of the spot size of about 1.25 μm. This experimental profile corroborates the numerical one (*i.e.* 1.25 μm) from figure 1c along x_0. Additionally, the absence of light scattering along the SU8 nanotube is a direct evidence of the low roughness of the outer surface of the nanotube, and the absence of morphological defects. The presence of a diaphragm and a beam-splitter along the optical path of the vertical analysis/imaging setup allowed the selection of the collected area (roughly 5x5

μm) on the sample towards a spectrometer. Figure 4e presents the spectrum of the microlensed lobe light as well as the spectrum of the propagative spot collected by focusing the vertical bench. The similarity between both spectra confirms the full waveguiding behavior of the SU8 polymer nanotube. This efficient propagation has been also established under IR laser injection. Based on our previous theoretical works [11] and considering the lateral size of the nanotube, only a single-mode HE_{11} is expected to propagate here.

5.2 Coupling phenomena

The light injection is particularly challenging at the nanoscale, thus deserving a specific study. First, a home-made Labview interface was implemented on the experimental setup. The goal was to draw a map of the propagative spot intensity as a function of the microlensed position. The intensity of the propagative spot is determined by summing the intensity of a 60x60 pixels area centered on it [27]. The transversal mapping of the spot intensity has been recorded for four x-positions of the microlens a) x$\cong$ 0μm, b) x= 1μm, c) x= 2μm, and d) x= 3μm. At each couple of coordinates (y,z) of the microlens, the intensity of the spot is recorded and corresponds to a point on the map presented on the figure 5. Thereby, these maps represent the evolution of the intensity of propagative spot for each couple of coordinates (y,z) at fixed x-position. They clearly highlight an optimized position of the microlens with a more adequate (yellow color) efficient optical coupling and so a more intense propagative spot. The

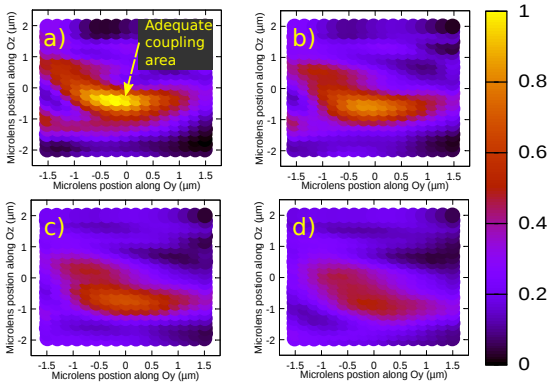

Fig. 5 Transversal (Oyz) intensity maps of propagative spot light at a) x$\cong$ 0μm, b) x=1 μm, c) x=2 μm and d) x=3 μm.

efficient coupling is directly proportional to the distance between microlensed fiber and nanotube, thus maximal for the smallest distance. This experimental observation corroborates the theoretical study presented above on figure 1d. It can be noted that the more efficient coupling is achieved in a volume of 0.6 μm^3 with a variation of less than 20 %. Thus, it allows a flexibility in the coupling process, which permits to properly estimate the optical losses into such 1D-nanostructures.

5.3 Optical Losses

The propagation behavior in SU8 nanotubes has been investigated. One of the most accurate method for evaluation of attenuation coefficient in waveguiding structures is the cut-back method [15]. It allows determining the intrinsic losses due to absorption, bending and scattering effects when light travels through the fiber. In this method, the power transmitted through a fiber is measured for several lengths and gives access to the attenuation coefficient α by Beer's law: $\alpha = \frac{10}{L_i - L_j} \log(\frac{P_j}{P_i})$ where L_i and L_j are sample lengths with $L_j < L_i$ and P_i, P_j the corresponding powers detected at the output of the fiber. By plotting the measured light power at the output of the SU8 nanotube *versus* propagation distances $(L_i - L_j)$, the attenuation coefficient α can be determined. The usual strategy to apply this method implies the detection of the transmitted power with a power-meter. 1D nanostructures based devices, the sub-micronic dimensions are not compatible with this detection tool. So we have adapted and developed a method derived from the cut-back process involving top view imaging. Indeed, the principle is based on the integration of the propagative spot intensity at the end side of the nanotube recorded on a 60x60 pixels area on the CCD camera for different lengths of nanotube. Once recorded for a first length, the nanotube is cut directly on the SiO_2 wafer by micromanipulation of a sharp tungsten probe and a second intensity can be recorded. For each length, the protocol of direct injection described previously was repeated, in order to optimize the efficiency of coupling between the microlens and the SU8 nanotube. It is noteworthy that the injected light conditions are not perturbed by the cutting step and thus allow an accurate comparison of the transmitted powers. In addition, the second key for reliable measurements is related to the cleaved endfacet of the nanotube that must be clean and sharp. These points were established by SEM imaging after cutting a SU8 nanotube, as shows on figure 6a. In addition, every propagative spots for the different lengths present the same intensity profile (see figure 4c), which confirms the quality of the cleaved endfacets. This study has been performed under red light (675 nm) for several nanotubes. Figure 6c gathers experimental results and show the expected exponential behavior. The analysis of these experimental data performed on 9 nanotubes and 24 propagation distances leads to a distribution of attenuation coefficients summarized on figure 6d, with an average value of 1.25 dB/mm. According to the measurement protocol described above, the discrepancy due to the positionning for coupling can be neglected. Such a dispersion is rather attributed to positionning and experimental variation of SU8 nanotubes such as structural defects or diameter varia-

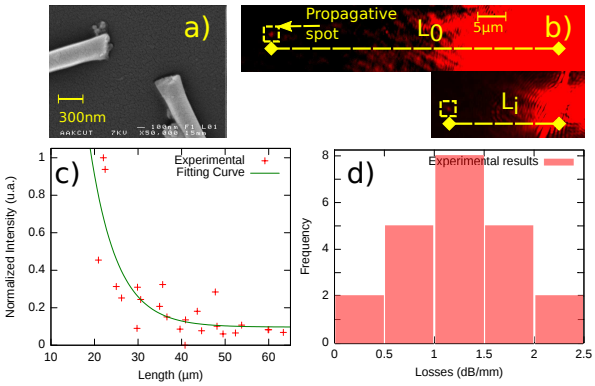

Fig. 6 a) SEM image of a clean cleaved endface of SU8 nanotube, b) top-views of fimages during waveguiding of laser light at different length. c) Intensity of propagative spot for different propagation distances and d) distribution of losses centered around 1.25 dB/mm.

tion. Regarding the origin of losses, without bending of the nanowaveguide, the attenuation coefficient α takes into account intrinsic losses due to absorption, scattering losses due to surface defects and losses due to the cladding of the nanotube (SiO_2 and air). Regarding, absorption mechanisms, it is minimized in our case because the SU8 polymer is transparent in the wavelength range [650-1000 nm][28]. Regarding the scattering losses, a previous theoretical study on silica nanofibers has shown that a small variation of roughness along a waveguide nanofiber induces a variation of refractive index and increases dramatically losses[29]. As mentioned, on figure 2c, the small roughness (about 5 nm) of the nanotube surface is expected to induce only a small scattering contribution. As presented in the theoretical study, the principal origin of losses in our system can be attributed to the SiO_2 wafer which induces a leaking effect and thus reduces the effective confinement. It can be noted that plasmon waveguides present losses of 400 dB/cm[30]. In previous work[14], scattering losses of SU8 nanotubes had been estimated around 150 dB/mm. This higher value was allocated to the measurement process (*i.e.* scattering), to a synthesis process not optimized. For comparison, SU8 microstructures exhibit losses of 1.7 dB/cm[31]. Thereby, this attenuation coefficient around 1.25 dB/mm is well consistent with the excellent characteristics of SU8 polymer for optical waveguides. Meanwhile, compared with micronic waveguides, SU8 nanotubes provides opportunities for developping highly compact photonic devices. The low-loss behavior demonstrated in this work can be extended to other types of broader perspectives for future nanophotonics, and should be a valuable reference for optical applications of nanofibers. In parallel, relative part of evanescent field may offer wider opportunities of the waveguiding SU8 nanotubes in applications such as chemical or biological sensors.

6 Conclusions and perspectives

Injection and waveguiding properties of nanotubes were investigated both numerically and experimentally. The SU8 photoresist for integrated photonics was used to elaborate the nanotubes by a template strategy. Direct injection in organic nanotubes has been demonstrated experimentally by the use of microlensed fiber showing final radius of curvature of 500 nm. This original injection approach is supported by FDTD simulation. This protocol can be extended to investigation of 1D-nanostructures and more generally to sub-micronic structures. A method derived from the cut-back protocol was developed to estimate the attenuation coefficient for the first time in SU8 nanotubes. A value of 1.25 dB/mm was measured. The origin of losses in this sub-wavelength waveguide has been addressed. Based on the simulation results, the limitation of light confinement by the substrate appears to be the main source of losses. The investigation of light propagation inside nanotube will allow a deeper understanding of the phenomena of modulation and guiding light in SU8 polymer nanostructures in more complex systems. These two features make polymer SU8 nanotubes a good candidate as building blocks for integrated nanophotonics and sub-wavelength optical probes for near-field interactions by their original optical properties.

7 Acknowlegments

The authors thank Jo Le Lannic and Francis Gouttefangeas for SEM characterization, Guillaume Raffy for FDTD study, Ludovic Frein and Steve Bouhier for helpful discussions and experimental assistance. J. Bigeon PhD is supported by the Lab-O-Mat french network between CNRS, Nantes University and Rennes 1 University, and Bretagne and Pays de la Loire Regions.

References

1 L. Tong, F. Zi, X. Guo and J. Lou, *Optics Communications*, 2012, **285**, 4641–4647.
2 B. Piccione, C.-H. Cho, L. K. v. Vugt and R. Agarwal, *Nature Nanotechnology*, 2012, **7**, 640–645.
3 F. Gu, X. Yin, H. Yu, P. Wang and L. Tong, *Optics Express*, 2009, **17**, 11230–11235.
4 Y. Xiao, C. Meng, P. Wang, Y. Ye, H. Yu, S. Wang, F. Gu, L. Dai and L. Tong, *Nano Letters*, 2011, **11**, 1122–1126.
5 M. A. Foster, A. C. Turner, M. Lipson and A. L. Gaeta, *Optics Express*, 2008, **16**, 1300–1320.
6 R. R. Gattass, G. T. Svacha, L. Tong and E. Mazur, *Optics Express*, 2006, **14**, 9408–9414.
7 A. Garreau, F. Massuyeau, S. Cordier, Y. Molard, E. Gautron, P. Bertoncini, E. Faulques, J. Wery, B. Humbert, A. Bulou and J.L. Duvail, *ACS Nano*, 2013, **7**, 2977–2987.
8 D. O'Carroll, I. Lieberwirth and G. Redmond, *Small*, 2007, **3**, 1178–1183.

9 V. R. Almeida, Q. Xu, C. A. Barrios and M. Lipson, *Optics Letters*, 2004, **29**, 1209–1211.

10 C. Zhao, Z. Tang, Y. Ye, D. Fan, L. Qian, S. Wen and G. Chen, *Optics Express*, 2007, **15**, 6629–6634.

11 D. Duval and B. Bêche, *Journal of Optics*, 2010, **12**, 075501.

12 J. Hu and C. R. Menyuk, *Advances in Optics and Photonics*, 2009, **1**, 58–106.

13 T. Khudiyev, E. Ozgur, M. Yaman and M. Bayindir, *Nano Letters*, 2011, **11**, 4661–4665.

14 N. Huby, J.L. Duvail, D. Duval, D. Pluchon and B. Bêche, *Applied Physics Letters*, 2011, **99**, 113302–1–113302–3.

15 B. E. A. Saleh and M. C. Teich, *Fundamentals of Photonics*, Wiley-Interscience, 2nd edn, 2007.

16 K. Huang, S. Yang and L. Tong, *Applied Optics*, 2007, **46**, 1429–1434.

17 H. Xin, Y. Li, X. Liu and B. Li, *Nano Letters*, 2013, **13**, 3408–3413.

18 B. Bêche, N. Pelletier, E. Gaviot, R. Hierle, A. Goullet, J. P. Landesman and J. Zyss, *Microelectronics Journal*, 2006, **37**, 421–427.

19 H. Liu, J. B. Edel, L. M. Bellan and H. G. Craighead, *Small*, 2006, **2**, 495–499.

20 A. F. Oskooi, D. Roundy, M. Ibanescu, P. Bermel, J. Joannopoulos and S. G. Johnson, *Computer Physics Communications*, 2010, **181**, 687–702.

21 S. Wang, Z. Hu, H. Yu, W. Fang, M. Qiu and L. Tong, *Optics Express*, 2009, **17**, 10881–10886.

22 S.-S. Wang, J. Fu, M. Qiu, K.-J. Huang, Z. Ma and L.-M. Tong, *Optics Express*, 2008, **16**, 8887–8895.

23 A. Coillet, B. Cluzel, G. Vienne, P. Grelu and F. de. Fornel, *Applied Physics B*, 2010, **101**, 291–295.

24 C. R. Martin, *Accounts of Chemical Research*, 1995, **28**, 61–68.

25 M. Steinhart, R. B. Wehrspohn, U. Gösele and J. H. Wendorff, *Angewandte Chemie International Edition*, 2004, **43**, 1334–1344.

26 D. Di Camillo, V. Fasano, F. Ruggieri, S. Santucci, L. Lozzi, A. Camposeo and D. Pisignano, *Nanoscale*, 2013, **5**, 11637–11642.

27 Y. Ma, X. Li, H. Yu, L. Tong, Y. Gu and Q. Gong, *Optics Letters*, 2010, **35**, 1160–1162.

28 K. K. Tung, W. H. Wong and E. Y. B. Pun, *Applied Physics A*, 2005, **80**, 621–626.

29 A. V. Kovalenko, V. N. Kurashov and A. V. Kisil, *Optics Express*, 2008, **16**, 5797–5806.

30 W. Wang, Q. Yang, F. Fan, H. Xu and Z. L. Wang, *Nano Letters*, 2011, **11**, 1603–1608.

31 B. Bêche, N. Pelletier, E. Gaviot and J. Zyss, *Optics Communications*, 2004, **230**, 91–94.